The Effect of Fly Ash Chemical Composition on Compressive Strength of Fly Ash Portland Cement Concrete

THESIS

Presented in Partial Fulfillment of the Requirements for the Degree Master of Science in the Graduate School of The Ohio State University

By

Matthew Chelberg, B.S.

Graduate Program in Civil Engineering

The Ohio State University

2019

Master's Examination Committee:

Dr. Lisa Burris, Advisor

Dr. Tarunjit Butalia

Dr. Abdollah Shafieezadeh

ABSTRACT

The objective of this study was to examine the influence of the bulk chemical composition of fly ash on the compressive strength of concrete. Results from the compressive strength tests of 181 concrete samples that used partial cement replacement with fly ash were used as data to create multiple linear regression models. These models were compared to a baseline model to predict the compressive strength of concrete based on bulk composition of the fly ash. Both statistical and experimental methods were used for verification. This study found that the new Selected model measuring w/c ratio, w/c ratio, LOI, and the bulk percentage of six metal oxides, was better able to predict concrete 28-day strength. It finds that the current ASTM limits for fly ash are insufficient to fully explain the strength of concrete utilizing fly ash and that a better set of measurements is needed to determine if a fly ash is acceptable for use in concrete for structural applications.

ACKNOWLEDGEMENTS

My advisor for a depth of knowledge and dedication to this endeavor. Anderson concrete for its contribution of fly ash and its dedication to the increasing understanding and knowledge. My parents for always encouraging me to learn and that I don't know my limits unless I push myself farther than I think I can. My girlfriend for helping me push through the hard times and always being there for me to rely on. Finally, to Ohio State for the opportunity to contribute to scientific inquiry.

VITA

May 2013 .....B.S., Civil Engineering,
The Pennsylvania State University
State College, PA

May 2015 to August 2017 .....Structural Engineer
M-Engineering
Westerville, OH

August 2017 to present .....Graduate student
Civil Engineering Department
The Ohio State University,
Columbus, OH

FIELDS OF STUDY

Major Field: Civil Engineering

Specialization: Structural Engineering

TABLE OF CONTENTS

LIST OF TABLES

LIST OF FIGURES

CHAPTER 1. INTRODUCTION

1.1 Research Problem Statement

Fly ash has been a supplementary cementitious material (SCM) used in the production of concrete for decades. Fly ash suitability for use in structural concrete is determined by many factors including its bulk chemical composition. This bulk chemical composition measurement is inadequate to determine the efficacy of fly ash and restricts the use of much of the produced fly ash. To increase the amount of useable fly ash, this research develops a statistical model, using the bulk chemical composition of fly ash, that can better determine the effects and quality of fly ash on the compressive strength of concrete. The objective of this study was to examine the influence of the bulk chemical composition of fly ash on the compressive strength of concrete.

1.2 Organization

In total, seven chapters are included in this thesis. Chapter one introduces the research project and lays out the objectives, scope, and significance of this research, while chapter two provides the background information. Chapters three and four describe the materials and methodology used to conduct the experiments. Chapters five and six present the results and a discussion of the analysis. Chapter seven presents the conclusions and lays out a path for future work.

CHAPTER 2. BACKGROUND INFORMATION

2.1 Overview of Concrete

Concrete is one of the most used building materials in the world. It has been used for millennia to construct many of mankind's most ambitious structural projects. Concrete's popularity is partially based on the ease with which it can be made. At its simplest, concrete is a mixture of fine aggregate (sand) and course aggregate (gravel), a binding paste (cement) and water. From these simple substances, a remarkably versatile material is made. Concrete is defined by its properties when in the hardened state.

2.1.1 Cement

The widespread global use of concrete has a severe environmental impact including a large-scale carbon footprint (Tait and Cheung 2016). Cement is the most energy intensive and costly component of concrete (Ahmaruzzaman 2010). Most of this comes from the energy used to mine, manufacture and transport cement, as well as the release of greenhouse gases such as carbon dioxide.

Today, there are many types of Portland cement, the most used binding paste, but the most common is ordinary Portland cement (OPC). The main chemical reaction in the manufacture of ordinary Portland cement is the formation of calcium silicates from calcareous and argillaceous materials, such as limestone or chalk (calcium carbonate) and clay or shale (made up of silicates). These raw materials are widespread globally, allowing for the easy manufacture of cement. As the raw materials are heated they break down into

their component oxides. Then, as the temperature increases, these combine into di- and tri-calcium silicate. This mixture, along with lesser amounts of metallic compounds (primarily iron and aluminum) from the clay, is called the clinker. A small amount of gypsum is added to the clinker which is then ground into a fine powder – the common cement used for many building projects. As seen in Table 2-1, the primary two compounds, tri-calcium and di-calcium silicate, make up the majority of the cement and are responsible for most of the compressive strength gain in concrete.

Table 2-1 Main Components of Portland Cement adapted from Mamlouk & Zaniewski 2006

Compound	Chemical formula	Common formula	Usual range by weight (%)
Tricalcium Silicate	3 (CaO) * SiO_2	C_3S	45-60
Dicalcium Silicate	2 (CaO) * SiO_2	C_2S	15-30
Tricalcium Aluminate	3 (CaO) * SiO_2	C_3A	6-12
Tricalcium Aluminoferrite	4 (CaO) * Al_2O_3 * Fe_2O_3	C_4AF	6-8

It is important to note that cement chemistry uses an abbreviated set of notations in order to shorten the typical chemical formulas used in the field: C = CaO, A = Al_2O_3, S = SiO, H = H_2O, F = Fe_2O_3.

2.1.1.1 Cement Hydration

Portland cement concrete uses the process of hydration to create concrete. The main process is the combination of cement particles and water (Mamlouk, M.S., Zaniewski 2006). These materials chemically combine with an accompanying change in phase and a change in energy level. The multiple compounds present in cement cause several chemical reactions to occur simultaneously. The most important of these are the hydration of tricalcium silicate (C_3S) and dicalcium silicate (C_2S).

The equation for the hydration of tricalcium silicate (C_3S) is:

Tricalcium silicate + Water → Calcium silicate hydrate + Calcium hydroxide

$$2\ Ca_3SiO_5 + 7\ H_2O \rightarrow 3\ CaO*2SiO_2*4H_2O + 3\ Ca(OH)_2 \quad (1)$$

The second dominant silicate in cement, dicalcium silicate (C_2S), undergoes a similar reaction, but the rate of reaction is slower.

Dicalcium silicate + Water → Calcium silicate hydrate + Calcium hydroxide

$$2\ Ca_2SiO_4 + 5\ H_2O \rightarrow 3\ CaO^*2SiO_2{}^*4H_2O + Ca(OH)_2 \quad (2)$$

The main product of the hydration of Portland cement is calcium-silicate-hydrate (C-S-H) which is formed when calcium silicates react with water. The stoichiometry or precise reactant/products mix of C-S-H is not well-defined (Mamlouk, M.S., Zaniewski 2006). As a result, the formula for calcium silicate hydrate is often written as C_x-S_y-H_z, or C-S-H for simplicity. The calcium-to-silicate ratio varies depending on many factors, including w/c of the mixture, and the precise mixture of phases present in the cement, and the amount of

C-S-H produced by either C_3S and C_2S is different. The other primary product of the cement hydration process is calcium hydroxide (CH). C-S-H develops strength and CH fills in gaps or voids.

2.1.1.2 Cement's Carbon Footprint

There are three main sources of anthropogenic emissions of carbon dioxide: (i) oxidation of fossil fuels, (ii) deforestation and other land-use changes, and (iii) carbonate decomposition (Andrew 2017). Cement is the largest source of the third category, carbonate decomposition. The two main ways that it produces carbon dioxide is the combustion of fossil fuels needed to heat the raw materials to the requisite high temperatures and the chemical reactions involved in making clinker. The decomposition of the $CaCO_3$ into oxides and the resulting emission of CO_2 is estimated as contributing 5% of the global anthropogenic CO_2 emissions and the entire cement process is estimated as contributing 8% to the global CO_2 emissions.

2.1.1.3 Composition

Since clinker production is the most energy-intensive and CO_2-emitting step of the cement-making process, reductions in the clinker/cement ratio (through use of clinker substitutes) can reduce energy use and CO_2 emissions. In the USA, the average clinker/cement ratio was most likely about 0.95 for much of the 20th century, possibly dropping to about 0.90 or slightly lower after about 1970. However, the International Energy Agency (IEA) recently estimated the global average clinker/cement ratio to be 0.65 (IEA, 2017). In China where almost 60 % of cement is produced, the clinker/cement ratio is currently below 0.60.

This is achieved by blending clinker with non-clinker compounds, the most common of which are blast furnace or steel slag and fly ash. Materials like these, that add volume to cement without a significant loss of properties, are called “pozzolans”. This term comes from ash deposits on the Pozzol volcano. Unlike clinker production, pozzolan additions typically do not need additional pyro-processing and therefore reduce the overall carbon footprint of the cement.

2.2 Overview of Fly Ash

Fly ash is a byproduct of coal burning during the process of generating electricity in a coal-fired power plant. It is the residue that is too fine and light to fall down to the ground and instead can stay airborne. Fly ash is between 85-95% of total weight of ash produced by coal combustion (Yao et al. 2015) with the remainder being bottom ash. These particles, considered waste by-products within the coal-burning industry, are collected and stored on site at the power plant. They are then either sold as a material for reuse or disposed of as industrial waste.

The reuse or upcycling of fly ash is environmentally beneficial and fly ash is used for many applications including acidic soil amelioration, as a chemical absorbent for toxic elements in industrial wastewaters, for the synthetization of zeolites and for catalyzation in industrial applications. It is also incorporated into ceramic pastes and geopolymer cement, incorporated into road building and, in terms of this research, as an SCM additive in the production of cement (Yao et al. 2015) (Hemalatha and Ramaswamy 2017).

Partial replacement of cement with fly ash has a positive effect on the environmental impact of the creation of concrete (Wang et al 2017), as well as other beneficial environmental impacts such as the reduction of:

- air pollutants (with its resultant health problems) inherent in the disposal of the fine particle sized fly ash and
- contaminants, such as arsenic, cobalt, chromium, nickel, antimony, titanium, vanadium and zinc metals, leaching into the water and soil (increasing soil pH) around fly ash disposal sites that affect crop production in those areas (Yao et al. 2015).

Annual production of fly ash was estimated at 500 million tons worldwide in 2010. (Ahmaruzzaman 2010) and more recent estimates has placed that number at approximately 750 million tons (Blissett and Rowson 2012).

2.2.1 Use in Concrete

Fly ash is used industrially both as a cementitious material and as a partial cement replacement (PCR) material. It also can serve as a fine aggregate in concrete (Khan, Castel, and Gilbert 2017) (Xu and Shi 2018).

The focus of this research is on the structural application of fly ash as a partial replacement component of concrete. In 2017, 38 million tons of fly ash was produced with only 36.83% (14 million tons) used in concrete with only 63.09% of fly ash was used in total (American Coal Ash Association 2017).

Using fly ash as a PCR has several benefits. In addition to the economical (it is a waste product) and environmental benefits, it adds structural and mechanical benefits to the resultant concrete:

- Fly ash's fine particle size increases the density of concrete and reduces concrete's permeability (Sumer 2012).
- It reduces concrete's heat of hydration which in turn reduces thermal cracking (Bouzoubaâ and Lachemi 2001).
- It can increase concrete's resistance to acid and sulfate attacks (Hemalatha and Ramaswamy 2017).
- It significantly reduces concrete shrinkage (Gesoğlu, Güneyisi, and Özbay 2009).
- The spherical shape of fly ash particle increases the fresh concrete's workability (Xu and Shi 2018).
- Class F fly ash increases the setting time (Nguyen et al. 2015).

The slow, but long-term strength gain from fly ash comes from the pozzolanic reaction with CH. The basic pozzolanic reaction process, in which calcium hydroxide is converted to C-S-H or C-A-H, is shown in Equations 3 and 4 (Shi and Day 2000). This reaction is beneficial to both strength and durability as it results in densification and increases in the density of the binder matrix (Saha 2018). While the compressive strength gain is slower and lower than a pure OPC concrete at 28 days, strength gain can show increases up to 180 days after curing (Saha 2018).

$$Y[SiO(OH)_3]^- + XCa^{2+} + (Z - X - Y)H_2O + (2X - Y)OH^- \rightarrow C_X{-}S_Y{-}H_Z \qquad (3)$$

$$2[Al(OH)_4]^- + 4Ca^{2+} + 6H_2O + 6OH^- \rightarrow C_4AH_{13} \quad (4)$$

Lower burning temperature in recent years in power plants has resulted in higher rates of unburnt coal remaining in the fly ash that is captured. Government standards, Loss on Ignition (LOI) test, specify the amount of unburnt carbon in fly ash that can be used in cement. Higher rates of LOI adversely affect the air entrainer, an additive that increases the air content of the hydrating concrete, or other additives in a concrete mix (Blissett and Rowson 2012).

2.2.2 Amorphous material in fly ash

Amorphous materials, meaning those without a clearly defined form, are typically non-crystalline substances, having a varied structure and chemical composition. Depending on its source, fly ash is comprised mostly of 50-90% glassy amorphous material, primarily aluminosilicious in nature, and a smaller percentage of crystalline structures (Aughenbaugh, Stutzman, and Juenger 2016). While x-ray diffraction quantifies the bulk fraction of the amorphous portion of fly ash, the individual glasses are difficult to identify, but identification would be useful in predicting the reactivity of fly ash as an additive.

2.2.3 ASTM Standards for Fly Ash in Concrete

The American Society for Testing and Materials (ASTM) creates standards of practice that are used in many industries including the construction industry. ASTM C618-19 is the current Standard Specification for Coal Fly Ash and Raw or Calcined Natural Pozzolan for Use in Concrete ("ASTM C618-19: Standard Specification for Coal Fly Ash and Raw or

Calcined Natural Pozzolan for Use in Concrete 1" n.d.). This standard determines the usability of fly ash that can be used in concrete and classifies the various types, based partially on the measurement of the combined cumulative amounts of three oxides in the fly ash chemical composition - silicon dioxide (SiO_2), aluminum oxide (Al_2O_3) and iron oxide (Fe_2O_3). However, this combined bulk composition measurement alone is not enough to explain the reactivity or compressive strength of fly ash pastes (Kim et al 2018) (Aughenbaugh, Stutzman, and Juenger 2016).

There are three designations for supplementary cementitious materials in the ASTM C618 standard - Class N, Class F and Class C.

> Class N is for natural pozzolans. It is a designation for raw or calcined natural pozzolans such as volcanic ashes or various minerals that require calcination like clays or shales. This classification is not going to be covered in this research and is outside its scope.
>
> Class F is fly ash produced by burning anthracite or bituminous coal (Hemalatha and Ramaswamy 2017). It has pozzolanic properties and has more unburnt carbon, resulting often in higher air entrainer requirements. It often does not have a large amount of reaction during the initial hydration of the cement (Hemalatha and Ramaswamy 2017), but instead begins to react after 28 and 90 days of curing..
>
> Class C is fly ash produced from burning lignite or subbituminous coal and has both cementitious as well as pozzolanic properties. This usually results in higher compressive strength for class C fly ash mixes than for class F. This even helps to

maintain the early strength of the concrete (Hemalatha and Ramaswamy 2017). The primary difference between Class F and Class C is the CaO percentage with the requirement that fly ash must contain more than 18% to classified as Class C.

The ASTM C618 standards dictates minimum or maximum requirements for many chemical and physical attributes that fly ash must conform to be used in concrete. These attributes are shown in Table 2-2.

Table 2-2 Characteristics of Fly Ash in ASTM C 618

Fly Ash Characteristics of ASTM C618	**Limits**	**Purpose**
(Al_2O_3 + Fe_3O_2 + SiO_2)*	> 50%	Chemical limits to predict performance
CaO*	>18% for class C	Chemical limits to predict performance, included in 2019 update to the specification
SO_3	< 5%	Ensure volumetric stability and typical hydration kinetics are not disrupted from excessive sulfate
Moisture content	< 3%	Ensure transportability and transfer to storage silos
Fineness (Max. % retained on No. 325 sieve)*	34%	Ensure material uniformity and standard strengths
LOI	< 6%	Limits on unburnt carbon to help reduce adsorption of air entraining agent

*indicates properties expected to influence strength development.

2.3 Analytical Model Criteria

The goal of the analytical model is to find the parameters of the fly ash that are best predictive of compressive strength in concrete. Linear regression is a common but powerful type of predictive analysis. It attempts to answer two basic questions:

- How well does an independent variable (or set of independent variables, in this case) do in predicting a particular outcome, the dependent variable?
- Which independent variable(s) is the most significant predictor of the outcome variable?
    - How does it impact the outcome variable? This is identified by the magnitude and sign of the beta estimates.

In this research, given the many variables that possibly influence the compressive strength, a multiple linear regression model was used.

CHAPTER 3. EXPERIMENTAL MATERIALS

The cement used in the experimental portion of this research was Fairborn Cement which is an ASTM class I Ordinary Portland Cement (OPC) meeting the ASTM C150 requirements.

Table 3-1 Oxide Content of the Cement

SiO_2	**Al_2O_3**	**Fe_2O_3**	**CaO**	**MgO**	**SO_3**
19.0%	4.5%	3.4%	62.4%	4.4%	3.1%

The sand used was obtained commercially from Quickcrete, similar to graded sand as specified in ASTM C778-17 and meeting the requirements (ASTM n.d.). This was used as fine aggregate in all batches of cement mortar. The size distribution is given in Table 3-2.

Table 3-2 Sand Gradient % Passing Compared to ASTM C778 Requirements

Sieve Size	% Passing of Fine Aggregate	% Passing of ASTM C778 "Graded Sand"
No.4	100.00%	100%
No.8	99.15%	100%
No.16	99.15%	100%
No.30	98.96%	96-100%
No.40		60-75%
No.50	53.24%	16-30%
No.100	3.22%	0-4%
No.200	0.19%	
Pan	0.00%	

The water used in this research was sourced from the Ohio State University water supply. The 2018 City of Columbus, OH Consumer Confidence Report (CCR 2018) stipulates that the annual water hardness for the Hap Cremean Water Plant which supplies the Ohio State University campus is 89 mg/l with a range of 74 - 111 mg/l. (1 ppm as $CaCO_3$ is equivalent to 1 mg/l). This is considered moderately hard water. The water comes from the Hoover Reservoir on Big Walnut Creek. This water was used in making all concrete mortar cubes.

Five fly ash samples were tested in this research as verification for the analytical models and the sample information is shown in Table 3-3.

Table 3-3 Fly Ash Sources, Type, LOI, and Chemical Composition from XRD Analysis

Fly Ash Sample	Fly Ash Type	Loss on Ignition	SiO_2	Al_2O_3	Fe_2O_3	CaO	MgO	SO_3	Na_2O	K_2O	P_2O_5	TiO_2
FA#2	F	0.51	67.84	20.98	3.05	2.41	1.31	0.18	0.63	1.73	0.27	1.56
FA#3	C	2.71	45.87	18.16	9.13	14	4.87	1.97	1.48	0.67	1.95	1.92
FA#4	C	2.63	44.78	18.63	6.78	15.56	5.32	3.04	2.32	0.53	1.52	1.5
FA#5	F	1.93	62.36	19.83	9.78	2.74	1.01	0.18	0.61	1.68	0.26	1.51
FA#6	unknown	2.21	64.64	20.91	5.78	3.14	1.1	0.18	0.64	1.74	0.27	1.57

The samples were tested for Loss on Ignition (LOI). LOI was determined by heating samples at 20 °C/min to 95˚C using a Mettler Toledo thermogravimetric analyzer in an inert nitrogen atmosphere. All the fly ash samples were determined to be within ASTM limits of 6% for LOI. The results are shown in Table 3-3.

ZnO (zincite), commercially obtained from Alfa Aesar, was added to all XRD samples of fly ash as an internal standard. It has a purity of 99.9% metals basis with a fineness of a 200-mesh powder.

CHAPTER 4. METHODS

The focus of this research was to create a statistical model of the compressive strength of concrete made from cement containing replacement fly ash. To do so, this research attempted to first analytically identify the chemical characteristics of the replacement fly ash that contribute to enhancing the compressive strength of the resulting concrete, then to experimentally validate the model.

The experimental validation was divided into two parts: the crystalline phase content of variously sourced samples of fly ash and the measurement of the compressive strength of the resulting samples of concrete. Crystalline phase content testing was performed using x-ray diffraction to determine the crystalline phase content of each of the fly ashes. Compression testing of samples of cement mortars made with each of the different fly ashes was then used to determine the stress in each sample at the point of failure.

Information was extracted from papers published in the academic literature to compare fly ashes composition and its relationship with the compressive strength of the concrete that it is in.

4.1 Experimental Methods

4.1.1 X-Ray Diffraction (XRD)

Traditionally, fly ash composition is expressed as bulk chemical composition, in particular the elemental oxide content. The chemical composition and phase content of fly ash varies based on the coal source and its minerology, the coal burning conditions and how the fly ash was collected. For this experiment, determining the crystalline phases of the fly ash was also necessary to determine the bulk chemical composition of each sample of fly ash.

Five samples of fly ash were analyzed using XRD crystallography testing to determine the crystalline phase content of fly ash. The phase content is the quantity and types of crystalline structure present in the fly ash. The fly ash samples were prepared, scanned, and analyzed to identify the crystalline phases present.

4.1.2 Sample Preparations

Sample preparations were similar to those used by Chancey et al. (Chancey et al. 2010). Each sample contained 90% fly ash by weight and 10% zincite. After passing through a #200 sieve, 0.900 g of fly ash was mixed with 0.100 g of 99.9% pure ZnO (Zincite) as a 10% by weight internal standard. Zincite is not present in the fly ash sample, so the addition of a known amount of zincite was used to calibrate the readings of the XRD to determine the comparative quantities of the other crystalline phases.

The fly ash and internal standard were ground together using a ceramic mortar and pestle and mixed with a non-reactive isopropanol solution to form a homogeneous slurry. The grinding both mixed the zincite and the fly ash and also ensured homogenous particle size. The sample was allowed to stand at room temperature to allow for all the isopropanol to evaporate.

Each sample was then transferred into a plastic, top-loaded XRD sample holder and manually compacted using a flat plate and razor blade to ensure that it was flush with the edge of the container and remained in place when subjected to rotation within the diffractometer. This minimized the surface texture variation and, only using vertical force, minimized artificial preferential alignment of the crystalline structures in the sample.

4.1.3 Data Acquisition

X-ray diffraction is a method of analysis that directs x-rays at a sample of fly ash at a specific range of angles and measures how much of the beam was diffracted at each angle. Different crystalline structures diffract at specific angles and, by recording the intensity of x-rays diffracting and matching the locations of peaks, the specific phase content can be obtained.

After data collection, the profile of measurements of the intensity of diffraction at a spectrum of angles is then compared to the known distributions of various crystalline structures to determine the amount of each structure present in the test sample. The XRD data was collected using a Bruker D8 Advance Powder diffractometer operating at 40 kV and 40 mA with a 1600 W copper x-ray source (producing Cu Kα radiation) with a flat plate reflection Johansson optics setting of 6 mm exit slit, a 0.2mm focus slit, and a 0.6mm divergence slit. The sample was rotated at 30 rpm and scanned from 5^{o} to 60^{o} of 2θ in rotation increments of 0.0197^{o} with 1 second dwell time. Each sample was scanned for approximately 50 minutes.

4.1.4 Qualitative data analysis

Qualitative analysis of the data was performed using the Profex software program. The shape of the diffraction curve, which includes the base hump of the amorphous material, was identified and analytically fit. The possible crystalline structures in fly ash were identified, and these standards were compared with the experimental XRD results to determine the actual crystalline structure of each fly ash source, allowing for the determination of the bulk chemical composition of each fly ash sample. The fly ash

reference phase structure files were obtained from the National Institute of Standards and Technology (NIST) website. The minerals present are identified manually and then optimized by the Profex software. This information was matched with observed diffraction peaks. Rietveld analysis of the experimental spectra was performed using the software, in order to determine the phase composition of each of the samples.

After performing the Rietveld analysis of fly ash phase content, the internal standard was identified as 10% of total material to determine the amount of each other material present. The remaining material with no peak data was then identified as amorphous, having no consistent crystal structure. This amorphous material will appear in the graphed data without the peaks that manifest from regular crystal structures.

The chemical composition of the amorphous content of the fly ash could not be determined by the XRD because it has no definitive and uniform crystalline structure. The chemical composition was estimated using the data compiled by Ward and French, 2006 (Ward and French 2006). Ward and French analyzed two sets of fly ashes, distinguished by the location from which they were obtained. Using x-ray fluorescence spectrometry and XRD, an inferred chemical composition of the amorphous content of the fly ash was determined. In this research, the percentage of the amorphous material experimentally computed was compared to Ward and French's analyzed sets and an estimated chemical composition was determined.

4.1.5 Mix Design and Sample Preparation

Using the same five fly ashes that were characterized using XRD, five batches of standard 2 inch by 2 inch by 2 inch specimen cubes of cement mortar were used to determine the

compressive strength. Following ASTM C109-16a and ASTM C305-14 (ASTM, n.d.) mixing procedures, for each fly ash sample.

The molds were kept in a moist curing environment for 24 hours for initial hardening. Then, after removal from the molds, the mortar cubes were stored prior to testing again in a moist curing environment maintained at 100% relative humidity, and 72 +/- 2C. Compressive strength was tested after 1, 3, 7 and 28 days of curing. Strength gain is anticipated to continue beyond 28 days and tests will be performed at 56 and 90 days. These tests, however, will be outside the scope of this report.

Table 4-1 The Mix Proportions of Mortar Cubes

Cement Mortar Batch Weights		
Material	**Weight (g)**	**% of Total Weight**
Sand	2035	66.27%
Ordinary Portland Cement	370	12.05%
Fly Ash	370	12.05%
Water	296	9.64%

4.1.6 Compression Testing

Compression testing of cement mortars was used to determine the stress in the material at the point of failure. This is performed on specimens at particular times to observe the accumulated strength at that time. For this research, the typical strength at twenty-eight days is of primary concern but tests at 1, 3 and 7 days were also conducted.

The compression test is performed by applying an even force or pressure across the cross section of the cement mortar cube. This is performed on specimen cubes of standard dimensions. As pressure is applied, the stress level within the specimens rises. Pressure is applied until the specimen is crushed. The maximum stress level is recorded. This is performed for each specimen on three cubes on each testing day and the results are averaged per specimen per testing day.

The cement mortar cubes were tested for compressive strength using the procedures outlined by ASTM C 109. The cubes were placed into the testing machine, a Forney compression machine, model F-250-VFD-MP with a 250,000 lbf. capacity. The machine settings included a 75% break percentage, 75 psi/second ramp rate and a pre-load of 100 lbf. Three samples from each batch were tested on each test day and the results were averaged.

4.1.7 Fly Ash Replacement Percentage

While a fly ash replacement percentage is typically 10–35%, in order to maximize the effects of the differences in the fly ash composition, a cement mortar containing 50% by weight of fly ash was used.

This percentage is in line with a study at the National Institute of Standards and Technology (NIST) to evaluate the early age strength development of concrete (Bentz 2010). A 50% replacement should have a lower overall compressive strength than a smaller replacement ratio, but with the goal of investigating the comparative difference of various fly ash sources, not an absolute value of the compressive strength, this will allow for the maximization of it.

4.2 Analytical Predictive Model

An extensive review of the datasets on fly ash replacement published in peer reviewed research journals was undertaken. A detailed Excel datasheet was assembled, and a linear regression model was created. In this research, the dependent variable of interest is the 28-day compressive strength of concrete made with fly ash and the independent variables include ten oxides in the cement and the water/cement, water/binder ratio, fly ash replacement percentage and LOI.

4.2.1 Data Acquisition

The dataset used in the regression formula was generated from published, peer-reviewed academic journal papers. Only papers that contained all of the following parameters were used:

- the 28-day compressive strength of the concrete,
- the chemical (oxide) composition of the fly ash,
- the water to cementitious material ratio (or information so that it could be calculated),
- the cement replacement ratio with fly ash and
- the LOI.

In addition, to minimize variations from materials other than fly ash, only research papers that used type I/II cement were included. For papers that used cubic test samples for compressive strength instead of cylinders, a conversion factor of 0.87 was used to normalize the values per ASTM C39/C39M ("ASTM C39/C39M - 05: Standard Test Method for Compressive Strength of Cylindrical Concrete Specimens" 2005). This

normalization was common for data from international papers. Both Class F and Class C fly ashes were used in the literature studies.

4.2.2 Model Selection

Linear models are made to have the smallest sum of errors in each parameter and to explain the variance. A multiple linear regression (MLR) model of the form:

$$Y' = \beta_o + \beta_1 * X_1 + \beta_2 * X_2 + \cdots + \beta_n * X_n \quad \textit{Equation 4-1}$$

where:

Y' = the predicted value of dependent variable

X_i = the value of each independent variable from n=1 to i

β_i = the coefficient for the independent variable (a measure of the influence)

Models with different combinations of independent variables were constructed to find the best version. One measurement of the best model is the R^2 value. It measures the amount of the variance that is explained by the model. These can be compared to show the difference in the effectiveness of each model. An Analysis of Variance (ANOVA) test for each model was performed to find the best coefficients and the confidence or P-values of each independent variable.

4.2.3 Validation of Model

Two things were searched for with the model. First, the developed model was used to explain the variation in compressive strength from the fly ash. Second, the model was used to find the most influential variables of the chemical composition of fly ash. Using the

software RStudio, linear models were created. The data was analyzed using the programming language R.

To determine which independent variables have a linear association with the dependent variable the null hypothesis, H_0: $\beta_I = 0$ i.e. if the linear coefficient is zero and there is no linear correlation. The alternative hypothesis, H_A: $\beta_I =/= 0$, i.e. that a linear association does exist is accepted if the P-value, a measure of probability, is less than a cut off value. Due to the number of variables, a confidence level of 99% was used to determine if the parameter is statistically significant ($P < 0.01$).

Mean squared error is a way to measure how large the error is in any predictive linear regression. The linear regression in this research uses a least squares method to determine the closest fit. That means that the equation that produces the least amount of error is the selected regression formula, given a set of independent variables.

4.3 Chapter Summary

In this chapter, the methods of both the experimental and analytical portions of the study were explained. The experimental portion of the study was made up of XRD scans to obtain the bulk chemical composition of the fly ash samples, and compression testing at twenty-eight days of mortar cubes that contained those fly ashes as an SCM. The analytical portion of the study explained the criteria for collecting data for use in the analytical models and the process used to create and select the best models.

CHAPTER 5. RESULTS

5.1 Analytical Model Results

The focus of this research was to identify the chemical characteristics of fly ash that significantly affect the compressive strength of cement. To that end, based on a literature review of papers with datasets that met the stated requirements, an integrated dataset of 53 fly ashes with a corresponding 181 different compressive strength test observations was created (see Appendix A). Figure 5-1presents a graphical representation of the fly ashes in the integrated dataset. The values were calculated by averaging the percentage by weight of the oxides in that dataset.

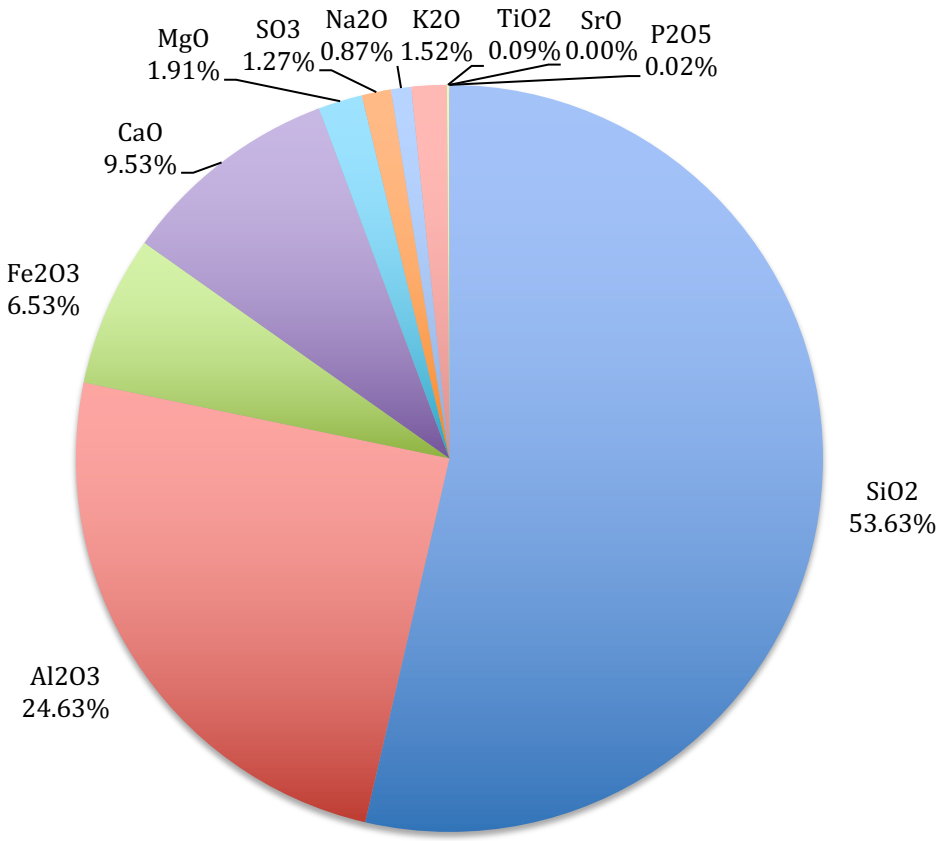

Figure 5-1 Average Bulk Chemical Composition of Integrated Dataset (Citations are in Appendix A)

For any given fly ash in the integrated dataset, multiple compressive strength test observations may exist with values based on differing variables such as the water/cement ratio and the replacement rate of cement. Each observation is a unique compressive strength data point of a concrete for a given fly ash. Utilizing this integrated dataset, a model of the fly ash characteristics that impact concrete's compressive strength was then created using a multiple linear regression model.

5.1.1 Best Model Determination

The goal of this research is to produce a model that best explains the data using as few parameters as possible. This led to two criteria to evaluate potential models: (a) how well a model fits the data and (b) how complex a model is, as measured by the number of independent variables – high fidelity and low complexity.

The number of independent variables considered is 14. Given this number of variables, every possible subset of the parameters is a potential model, therefore the total number of possible models is 2^{14} or 16,384. All possible models were systematically explored and ranked according to several measures including:

- R^2 (the measure of the variance/fidelity that is explained by the model),
- R^2_{adj} and
- BIC, Bayesian Information Criterion, is a combined measure of the complexity and fidelity.

After analysis, using both R^2 and R^2_{adj}, the recommended models were found to be weighted towards always including every parameter, even if they were not statistically significant. These models are of maximal complexity, therefore inappropriate for this research's purposes. A method of finding a model using a more balanced approach was required.

The criteria then used was to evaluate and rank the methods using BIC, which is a standard method for finding a model that balances the two competing imperatives, to fit the data well and to use a reasonable number of independent variables. BIC is calculated with the equation:

$$BIC = n \times ln(SSE_p) - n \times ln(n) + [ln(n) \times p] \quad Equation\ 5\text{-}1$$

where:

n = the number of observations

p = the number of variables

SSE_p = sum of squared errors for variables, p

All 16,384 models were sorted by their BIC value with the 14 lowest valued models highlighted in Figure 5-2 for closer examination.

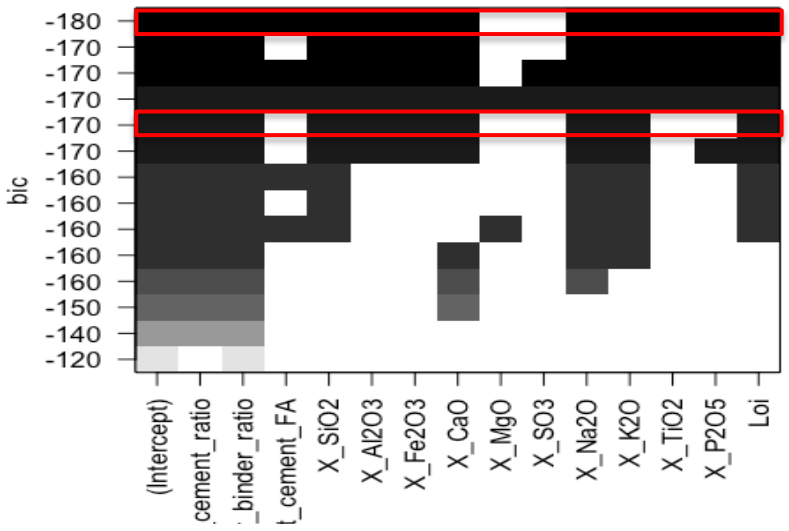

Figure 5-2 Comparison of models ranked by BIC method with the included parameters shaded in. Highlighted models are the BIC (upper) and Selected (lower) models.

5.1.2 Model Selection

After initial analysis, three models were selected for a detailed analysis.

5.1.2.1 ASTM Model

The first model was based upon the chemical requirements dictated by ASTM C618. ASTM C618 specifies the chemical requirements of fly ash for use in concrete. A key requirement is the minimum percentage of the combined presence of three oxides, silicon dioxide (SiO_2), aluminum oxide (Al_2O_3) and iron oxide (Fe_2O_3). Using this requirement, a control model based on the sum of SiO_2, Fe_2O_3, and Al_2O_3. for use in structural concrete, was established which could be used to compare the effectiveness of other models developed. Four other independent variables were included in the regression – the LOI, water/cement ratio, water binder ratio, and cement replacement ratio. The ASTM model only takes into account the information required by the ASTM C618 standard.

5.1.2.2 BIC Model

The second model was based strictly on the BIC test. The best model has the lowest BIC value (the values shown in Figure 5-2 are all negative) and it only excludes two parameters, MgO and SO_3. This model was named the BIC model.

5.1.2.3 Selected or non-P_2O_5 Model

After reviewing the results from the minimized BIC data, a third model was also compiled. In the BIC results of the fourteen lowest valued models, the coefficient for P_2O_5 appears to be an outlier in the models. It has a large influence on the predicted compressive strength. Holding all other variables constant, a one percent increase in P_2O_5 results in a more than a 100 MPa increase in the compressive strength of the concrete. Based on published results, this seemed unrealistic as a true predictor. The low number of fly ashes in the integrated

dataset that contained P_2O_5 might explain the out-sized level of influence that those data points had on the model.

In order to mitigate this, the P_2O_5 variable was determined to be non-representative and was removed from the model. This led to a new ranking of models in which the set of variables (not utilizing P_2O_5) with the lowest BIC was selected. This model was named the Selected model.

When the P_2O_5 variable was removed, it was shown that TiO_2 and the cement replacement percentage were found to no longer be statistically significant, so they too were removed, leaving only variables that are significant to a 99.9% level of confidence (w/c ratio, w/b ratio, LOI, % SiO_2, % Al_2O_3, % Fe_2O_3, % CaO, % Na_2O, % K_2O).

5.1.3 Model Evaluations

5.1.3.1 K-Fold Cross Validation

An issue to be addressed is the need to know if a regression model is generalizable beyond the data set that was used to create it. One method would be to test the model on a new independent data set, but frequently no such data set exists. An alternative method involves partitioning the data set into a training or model building set to develop the model and then comparing the predictive ability of the model to the remainder of the data set, the test set. The prediction errors (difference between the test set and the training set predictions) are calculated and summarized as the mean squared prediction error (MSPE). The K-fold cross validation method is used to measure the reliability of a model.

Each selected model was subjected to a K-fold cross validation. For example, the data could be 90% training set and 10% held back to be the test set. This is then repeated K times, with K being the number of training set/testing set separations.

For the model evaluations, the K-fold value was set to 40, splitting the data set into 40 parts and testing each part against all the others and measuring the difference between the mean squared error (MSE) and the mean squared predictive error (MSPE). The MSE indicates the total amount of error from the predicted values and the MSPE indicates the error in the test or validation data set compared to the training set. The difference between these numbers indicates how reliable the model is. The results are displayed below in Table 5-1.

Table 5-1 K-Fold MSE, R^2 and MSPE Results for Each Model

Model	**MSE**	**MSPE**	**MSPE - MSE**	**R^2**
ASTM	131.67	147.58	15.91	**0.6333**
BIC	97.78	125.72	27.94	**0.7386**
Selected	108.49	133.25	24.76	**0.7048**

While the ASTM model has the lowest difference between MSE and MSPE, it also has the highest MSE indicating that it has the lowest accuracy of the three models, but also the highest consistency when predicting. The BIC model had the lowest MSE indicating a high amount of accuracy to the overall data set, but also the greatest difference between the MSPE and the MSE making it the least consistent at prediction. That leaves the Selected model in between the other two on both counts. This does not indicate a clear best model so additional verification was needed.

5.1.3.2 Experimental Validation

A second way to validate each model was to test its predictive ability using experimental data. To do this the values of same variable that the model uses must be found. The XRD experimental data was used determine the chemical composition of each of the sample fly ashes. This data was combined with the other four independent variables to establish the complete fourteen independent variables dataset for each sample fly ash. This data was input into each of the three models and a predicted compressive strength was calculated. This predicted compressive strength was then compared to the actual experimentally determined compressive strength. The closeness of the comparative results was used as a tool for judging the validity of each model.

5.2 Chemical Composition of Experimental Fly Ash

In order to use the compressive strength experimental data as a verification test of the models, the chemical composition of the sample fly ash samples was established using XRD analysis.

5.2.1 XRD Results

5.2.1.1 Fly Ash Crystal Phase Content Result

The XRD results indicate the presence of crystal structures present in the fly ash as well as the amount of fly ash that is amorphous in nature. The results are displayed below in Table 5-2.

Table 5-2 XRD Crystalline Phase Content of Fly Ash Samples (% by Weight)

Crystal Phase	FA#2	FA#3	FA#4	FA#5	FA#6
Magnetite	0.49	0	0	4.55	2.00
Gehlenite	0	8.15	7.35	0	0
Mullite	6.39	0	4.82	5.50	5.10
Quartz	9.72	10.51	13.21	6.26	6.38
Lime (CaO)	0	0.65	0.84	0.41	0
Periclase (MgO)	0.26	2.14	2.39	0	0.05
Hematite	0	1.49	0.81	2.75	1.20
Mayenite	0	2.26	2.98	0	1.08
Merwinite	0	13.32	16.85	0	0
Mirabilite	0	2.93	4.95	0	0
Stratlingite	0	0	0	0	0.48
Amorphous	83.14	58.60	45.80	80.53	83.72

5.2.1.2 Fly Ash Experimental Amorphous Oxide Content

From the known chemical make-up of the crystal formulas, the amount of each oxide present in each fly ash was obtained, with the exception of the amorphous content. An estimate, based on the examination of amorphous content described by Ward and French (Ward and French 2006), was used to find the amorphous content of the fly ashes. Ward and French used the differences between the bulk chemical composition obtained with X-ray fluorescence and the detected crystal phases found in their XRD analysis to find the bulk composition in the amorphous content. The average results of their two groups are expressed in Table 5-3.

Table 5-3 Average Estimates of Amorphous Content of Fly Ash (Ward and French 2006)

Oxides	**Low Amorphous Content Percentages (Group A)**	**High Amorphous Content Percentages (Group B)**
% Amorphous	54.6	69.22
SiO_2	48.925	67.74
Al_2O_3	3.275	1.88
Fe_2O_3	24.075	19.72
CaO	12.95	3.08
MgO	1.775	1.26
SO_3	3.6	2.9
Na_2O	0.35	0.76
K_2O	1.15	2.08
P_2O_5	3.325	0.32
TiO_2	0.55	0.22
TOTAL	99.975	99.96

In the fly ash samples tested in this research, there were three high amorphous content fly ashes and two low amorphous content fly ashes. The amorphous content was assumed to be consistent with the low and high amorphous content groups described by Ward and French (Ward & French, 2006)

5.2.1.3 Total Crystalline Phase Content & Amorphous Oxides

Using both the experimental XRD results and the amorphous estimates based on the Ward and French experiments, the bulk oxide content of five fly ashes samples used in this research was determined. The total combined results are laid out below in Table 5-4.

Table 5-4 Total Bulk Oxide Content from XRD Phase Analysis and Amorphous Estimate (% by Weight)

Oxides	**FA#2**	**FA#3**	**FA#4**	**FA#5**	**FA#6**
SiO_2	67.84	45.87	44.78	62.36	64.64
Al_2O_3	20.98	18.16	18.63	19.83	20.91
Fe_2O_3	3.05	9.13	6.78	9.78	5.78
CaO	2.41	14.00	15.56	2.74	3.14
MgO	1.31	4.87	5.32	1.01	1.10
SO_3	0.18	1.97	3.04	0.18	0.18
Na_2O	0.63	1.48	2.32	0.61	0.64
K_2O	1.73	0.67	0.53	1.68	1.74
P_2O_5	0.27	1.95	1.52	0.26	0.27
TiO_2	1.56	1.92	1.50	1.51	1.57
TOTAL	99.97	100.03	99.98	99.96	99.97

5.3 Model Predictions Based on Experimental Dependent Variables

The resulting oxide percentages, in combination with the coefficients found in the linear regression models, were used as the values of the independent variables in each analytical model, which were used in turn to predict the compressive strength of each fly ash sample. Table 5-5 shows the computed regression coefficients for each of the models investigated.

In this regression models, as a result of the generation of negative oxide coefficients (with the exception of P_2O_5), smaller magnitude coefficients result in greater strength gains. As each sample is composed of 100% oxides present at all times, an increase in one oxide results in reductions in other components. If a component with a coefficient of -1.0 is replaced by a component with a coefficient of -4.0, with all else remaining equal, the end result is a net increase in compressive strength equal to 3 MPa.

Table 5-5 Linear Regression Coefficients for Each Model

Variable Names	**ASTM Model**	**BIC Model**	**Selected Model**
Intercept	107.140952	308.90627	257.4553
w/c	-12.220781	-13.0438	-19.0877
w/b	-64.46175	-59.29452	-52.4868
replacement ratio	-0.1413731	-0.20333	N/A
SiO_2+Al_2O_3+Fe_2O_3	-0.2816752	N/A	N/A
SiO_2	N/A	-2.29306	-1.9388
Al_2O_3	N/A	-1.97488	-1.431
Fe_2O_3	N/A	-3.01627	-2.0921
CaO	N/A	-2.64252	-2.0117
Na_2O	N/A	-6.73681	-4.6923
K_2O	N/A	-3.86217	-2.6972
TiO_2	N/A	-13.7874	N/A
P_2O_5	N/A	107.99604	N/A
Loss on Ignition	-1.8958547	-4.34194	-4.0981

The full equation for the Selected model is:

$$Y = 257.4553 + (-19.0877)*(\text{w/c ratio}) + (-52.4868)*(\text{w/b ratio}) + (-1.9388)*(\%\ SiO_2) + (-1.431)*(\%\ Al_2O_3) + (-2.0921)*(\%\ Fe_2O_3) + (-2.0117)*(\%\ CaO) + (-4.6923)*(\ Na_2O) + (-2.6972)*(\%\ K_2O) + (-4.0981)*(\%\ LOI) \quad (5)$$

Table 5-6 shows the computed P-values for each analytical model's coefficients (w/c ratio, w/b ratio, LOI, % SiO_2, % Al_2O_3, % Fe_2O_3, % CaO, % Na_2O, % K_2O). The smaller the P-value is, the higher the probability that it is significant.

Table 5-6 P-values for the Coefficients in the Analytical Models.

Variable Names	**ASTM Model**	**BIC Model**	**Selected Model**
Intercept	< 2e-16 ***	3.77e-14 ***	2.26e-11 ***
w/c	0.00328 **	0.000508 ***	4.65e-13 ***
w/b	7.11e-14 ***	8.08e-15 ***	1.29e-14 ***
replacement ratio	0.09276 .	0.015668 *	N/A
SiO_2+Al_2O_3+Fe_2O_3	0.00121 **	N/A	N/A
SiO_2	N/A	6.79e-08 ***	4.82e-06 ***
Al_2O_3	N/A	4.41e-07 ***	4.04e-05 ***
Fe_2O_3	N/A	7.54e-07 ***	4.19e-05 ***
CaO	N/A	6.07e-07 ***	9.26e-05 ***
Na_2O	N/A	1.18e-07 ***	2.24e-06 ***
K_2O	N/A	1.27e-06 ***	0.000431 ***
TiO_2	N/A	0.002351 **	N/A
P_2O_5	N/A	4.61e-05 ***	N/A
Loss on Ignition	0.03143 *	6.76e-06 ***	2.56e-05 ***

R^2	**0.6333**	**0.7386**	**0.7048**

Significance codes: '***' > 0.001, '**' > 0.01, '*' > 0.05, '.' > 0.1

Applying all of the experimental independent variable data to each of the three models resulted in a predicted fly ash compressive strength value, listed in Table 5-7.

Table 5-7 Predicted Compressive Strength of Sample Fly Ash Mortar Cubes

	ASTM (MPa)	**BIC (MPa)**	**Selected (MPa)**
FA#2	33.22	41.77	23.98
FA#3	34.32	214.33	24.42
FA#4	35.31	173.97	24.44
FA#5	30.50	29.40	15.93
FA#6	30.15	31.70	16.10

5.4 Compression Testing Results

To validate each models predictive capability, experimental compression strength testing results were measured for mortar cubes at times ranging from 1 day to 28 days and are given in Table 5-8, Figure 5-3 and Figure 5-4.

Table 5-8 Compressive Strength of Fly Ash Mortar Cubes (MPa)

Sample #	1-day strength	3-day strength	7-day strength	28-day strength
FA#2	10.40	13.84	18.81	28.59
FA#3	2.67	16.85	23.69	31.89
FA#4	1.12	11.12	18.33	28.15
FA#5	5.78	11.53	14.60	16.81
FA#6	5.81	9.54	12.87	17.45

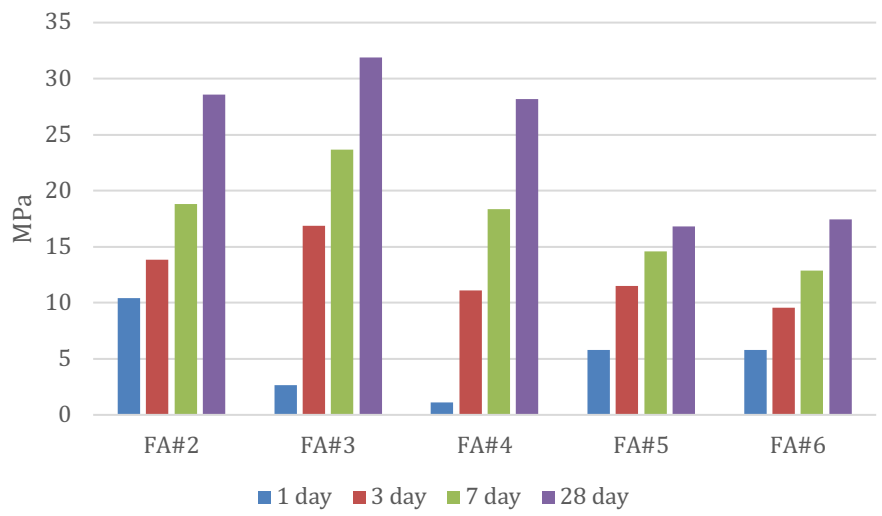

Figure 5-3 Compressive Strength Differences Over Time

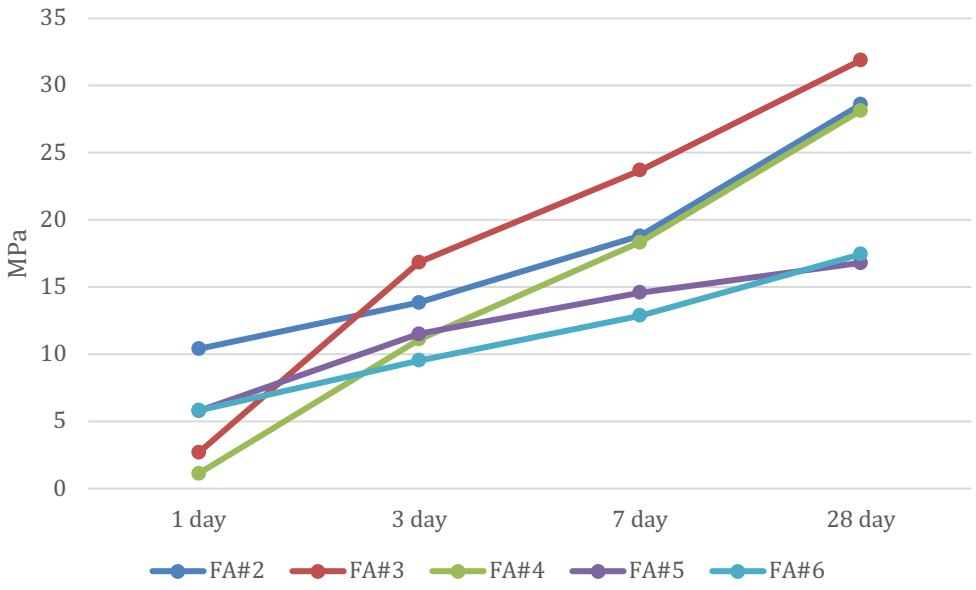

Figure 5-4 Compressive Strength Development Over Time

5.5 Predicted v. Experimental Compressive Strength

The experimentally determined compressive strengths were compared to the predicted compressive strengths for each model and are shown in Figure 5-5 and Figure 5-6. Figure 5-6 is the same set of data as Figure 5-5, but without the BIC model, for ease in showing the relative comparison between the two other models and the experimental data.

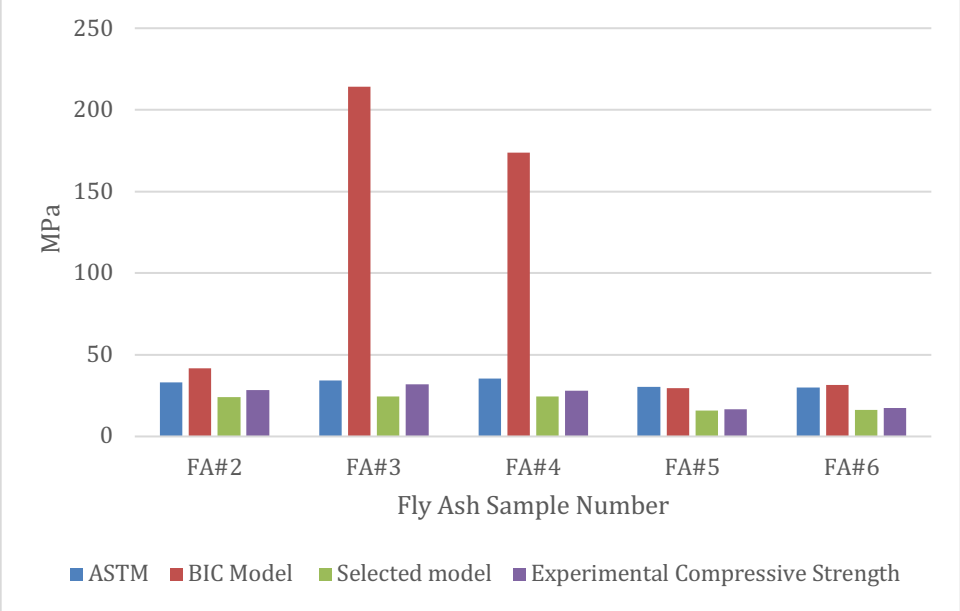

Figure 5-5 Comparison of the Compressive Strength Predictions from the Three Models and the Experimentally Measured Value

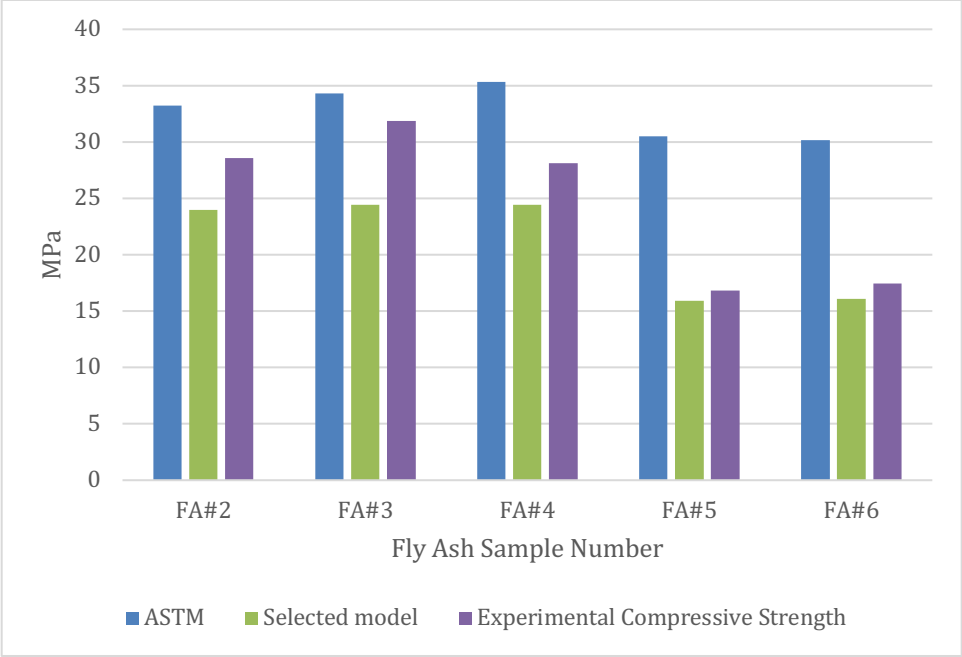

Figure 5-6 Comparison of the Compressive Strength Predictions from the ASTM and Selected Models and the Experimentally Measured Value

5.6 Amorphous Content v. Compressive Strength

The comparison of amorphous content in fly ash and the compressive strength is shown in Table 5-9. While not included as a variable in the prediction models it was expected to have an influence on the compressive strength. After the compressive test was performed, there was no strong correlation found between amorphous content and the compressive strength in the experimental results.

Table 5-9 Amorphous Content v. Compressive Strength

Sample #	**28-day strength (MPa)**	**% Amorphous Content**
FA#2	28.59	83.14
FA#3	31.89	58.60

FA#4	28.15	45.80
FA#5	16.81	80.53
FA#6	17.45	83.72

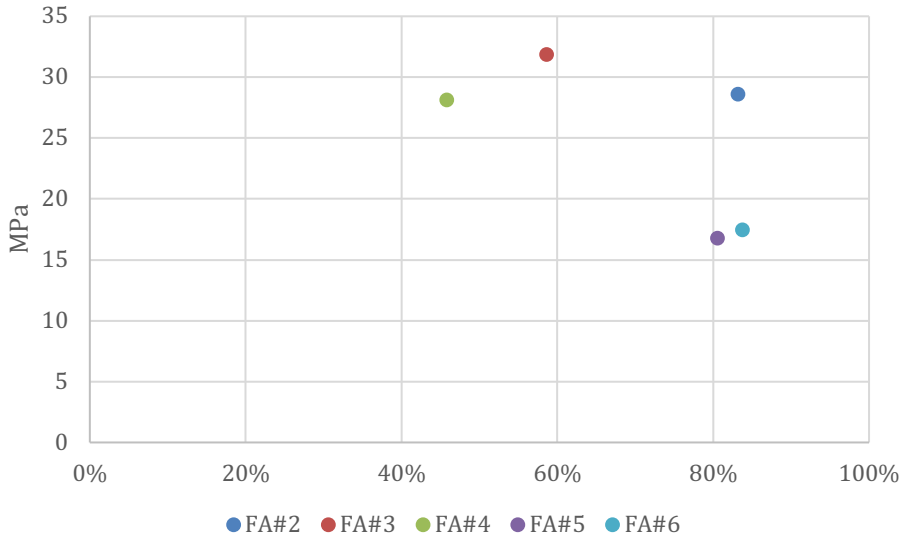

Figure 5-7 Amorphous Content v. Compressive Strength

5.7 Chapter Summary

In this chapter the three models were compared for effectiveness in predicting the compressive strength of concrete. They were chosen using the BIC number for each model and were verified both analytically with a K-fold cross verification and experimentally comparing predictions with results of compression tests of cement mortars with fly ash present. The results also show no direct correlation with the amount of amorphous content.

CHAPTER 6. DISCUSSION

The exploration of chemical and physical properties that explain the creation of compressive strength in concrete containing fly ash several models were investigated.

The ASTM model showed a large amount of error as denoted by the high MSE value. Although the differences between the MSE and the MSPE are small, meaning that the error does not increase by a significant amount, the error is already built into the model. This indicates that the current system is very consistent if not precise. The unreliability of the ASTM model indicates that it is missing important information and should not be used as a predictor of fly ash performance. The ASTM model is less effective at distinguishing changes in magnitude between the different fly ashes. It has a less powerful predictive nature due to the small number of predictors used, and the large amount of error, but it is relatively consistent in terms of error, meaning that the error doesn't increase much when predicting.

However, the BIC model fits this specific data set too closely. The MSE had the lowest error of the three models, but it comes at the cost of a higher increase in error when it was cross verified for prediction. This was further confirmed when examining its performance with the experimental data. The reason for this was largely from the coefficient for P_2O_5. Due to that coefficient there was a large discontinuity when predicting the fly ashes that had a significant amount of P_2O_5. The amount of phosphate caused it to give unreasonably large values. This seems to indicate that there is not enough data in the integrated dataset to give a conclusion on the effect of P_2O_5 in the fly ash samples. Its presence is a very small percentage even in the fly ashes that do contain it and it was only a small minority of fly

ashes that contained a detectable amount of it. The Selected model fit the experimental testing data the best. With it also being more accurate than the ASTM model and a more consistent prediction than the BIC model as tested by the K-fold cross validation, it was the best model. With the coefficients of all the oxides being negative, the smaller the magnitude of the coefficient results in it gaining more strength. Because there is 100% of the oxides present at all times an increase in one oxide reduces the others. If a coefficient is -1.0 and it replaces a percent with a coefficient of -4.0 than with all else remaining equal the end result is a net increase in compressive strength of 3.

Based on the chemical hydration processes known to occur between portland cement hydration products and pozzolanic materials, SiO_2, Al_2O_3, and CaO were initially hypothesized as components most significantly responsible for strength gain in the portland cement-fly ash mixtures. Shown in Equation 3, these components are the main components participating in the hydration reaction, which form the products C-S-H and the similar C-A-H (with the addition of aluminate). Since the primary generation of strength in concrete is derived from these products, the highest expected influence in chemistry comes from the SiO_2, Al_2O_3, and CaO required for the conversion of CH to C-S-H and C-A-H during the pozzolanic reaction of the fly ash and hydrated cement components.

The coefficients in the Selected model for Al_2O_3, SiO_2, and CaO are -1.431, -1.9388, and -2.0117, respectively, and represent the three most significant coefficients for compressive strength gain. These oxides were anticipated to be the most important chemical components in fly ash with respect to compressive strength gain, as they are known to participate in the pozzolanic reactions, leading to formation of more CH, C-S-H and C-A-H, and densification of the matrix. Coefficients associated with Al_2O_3 in both of the new models

indicate that Al_2O_3 has the highest effect on compressive strengths and should be measured independently of SiO_2 and Fe_2O_3. The Selected model developed by this research suggests that use of a higher alumina composition fly ash correlates with increased concrete mixture strength, thus a higher percentage of Al_2O_3 specifically in fly ash would be preferable for structural purposes, especially if included in high strength concretes. While Fe_2O_3 has the coefficient of -2.0921 which is close to the magnitude of SiO_2, and CaO, all three of these oxides are a second tier of strength generating oxides, well below that of alumina.

The rest of the oxides included in the Selected model (Na_2O, K_2O) have lower coefficients ranging from -2.6972 for K_2O to -4.6923 for Na_2O. However, as is shown in Figure 5-1, there is a smaller percentage of these oxides present in fly ash. They are not major contributors to the hydration reactions which might explain the lower coefficients. Due to the small number of data points of fly ashes with the more minor oxides (TiO_2, P_2O_5) the influence of these oxides is unclear and definitive conclusions about them cannot be made with only this data.

The coefficient for LOI was found to be an indicator of weaker concrete with a coefficient of -4.0981, demonstrating that as the amount of LOI increases it results in lower strength concrete. LOI was not anticipated to have a strong effect on the concrete compressive strength because the limitations that ASTM places on LOI were aim at preventing the unburnt carbon from reacting with air entrainer, not at ensuring generation of adequate strength. Air entrainer is only included in concrete mixes for durability reasons and the strength effect was surprising. This effect is likely due to the unburnt carbon present in fly ash that is measured by LOI being inactive in the hydration process. With an increase in LOI, a comparatively larger amount of inactive material replaces active reactants and reduces the strength of the binding matrix.

In the Selected model it is noteworthy that the cement replacement ratio was found to be a less likely predictor than including the water/binder ratio. Both of these measurements should contain similar information, but replacement ratio was found to have a higher P-value. This suggests that a more complicated relationship exists between cement and fly ash amounts in concrete that is not directly present in any of these models that could be addressed in future research.

It is important to note that these conclusions are all conditional within the range of values currently allowable for fly ashes in ASTM C618 but they do indicate that this is an incomplete way of measuring it. Even with the improvements in predictability that are found in this research, the R^2 values indicate that 30% of the variability in the concrete compressive strength is still unaccounted for by the models. This indicates that still unexplored factors should be investigated, such as phase content and the size of the fly ash particles.

CHAPTER 7. CONCLUSIONS

In order to determine the relative importance of chemical and physical properties and their relationship to generation of compressive strength, a model using published data in the academic literature and compared with results from five fly ashes was developed. This research also indicated that individual oxides affect concrete compressive strength gain. Measuring and utilizing more complete chemical makeup of the fly ashes and treating the various oxides as independent variables rather than as a group, will have a positive effect on the predictability of compressive strength.

Using both K-fold cross validation and experimental testing a model using information including w/c ratio, w/b ratio, LOI, and the percentage of the fly ash that was SiO_2, Al_2O_3, Fe_2O_3, CaO, Na_2O, and K_2O showed better predictive strength than the information in the ASTM C618. The selected model demonstrated a greater ability to predict differences in strength between fly ashes than the model based only on the information in the ASTM standard. The improved performance of the Selected model shows that the current ASTM measurement of the combined amount of SiO_2, Al_2O_3, and Fe_2O_3 is insufficient to explain the strength of fly ash in concrete.

CHAPTER 8. FUTURE WORK

This model selection process should be performed on a larger data set for more conclusive results and include additional parameters. Investigating the interaction between parameters such as the replacement percentage and the effect of the chemistry or phase content of the fly ashes could lead to additional reductions in the variation in predicted strength. At higher replacement percentages there is some indication that the effectiveness of the fly ash changes with respect to the strength of concrete, indicating a nonlinear relationship of replacement should be examined. Additionally, this research was limited to examining the effect on the 28 day strength but fly ash strength gain continues long after that and a model that can predict strength gain over time would be of even more use. Models could be developed that include reactivity measurements and particle sizes of the fly ashes or examine a larger data set that includes non-ASTM approved ashes. All of these have potential to further the understanding of fly ash's contribution to the compressive strength of concrete.

REFERENCES

Ahmaruzzaman, M. 2010. "A Review on the Utilization of Fly Ash." *Progress in Energy and Combustion Science*. https://doi.org/10.1016/j.pecs.2009.11.003.

American Coal Ash Association. 2017. "Production and Use Survey Report."

Andrew, Robbie M. 2017. "Global CO 2 Emissions from Cement Production." *Earth System Science Data*, 1–52. https://doi.org/http://dx.doi.org.kuleuven.ezproxy.kuleuven.be/10.5194/essd-10-195-2018.

ASTM. n.d. ASTM C778-17, Standard Specification for Standard Sand, ASTM International, West Conshohocken, PA, 2017, www.astm.org. Accessed March 19, 2019.

"ASTM C39/C39M - 05: Standard Test Method for Compressive Strength of Cylindrical Concrete Specimens." 2005. *ASTM International*, 1–8. https://doi.org/10.1520/C0039.

"ASTM C618-19: Standard Specification for Coal Fly Ash and Raw or Calcined Natural Pozzolan for Use in Concrete 1." n.d. *ASTM International*. Accessed March 19, 2019. https://doi.org/10.1520/C0618-19.

Aughenbaugh, Katherine L., Paul Stutzman, and Maria C. G. Juenger. 2016. "Identifying Glass Compositions in Fly Ash." *Frontiers in Materials* 3 (January). https://doi.org/10.3389/fmats.2016.00001.

Bentz, Dale P. 2010. "Powder Additions to Mitigate Retardation in High-Volume Fly Ash Mixtures." *ACI Materials Journal* 107 (5): 508–14.

Blissett, R. S., and N A Rowson. 2012. "A Review of the Multi-Component Utilisation of Coal Fly Ash." *Fuel*. https://doi.org/10.1016/j.fuel.2012.03.024.

Bouzoubaâ, N., and M Lachemi. 2001. “Self-Compacting Concrete Incorporating High Volumes of Class F Fly Ash: Preliminary Results.” *Cement and Concrete Research* 31 (3): 413–20. https://doi.org/10.1016/S0008-8846(00)00504-4.

Burris, Lisa E., and Kyle A. Riding. 2014. “Diffusivity of Binary and Ternary Concrete Mixture Blends.” *ACI Materials Journal* 111 (4): 373–82. https://doi.org/10.14359/51686826.

Chancey, Ryan T., Paul Stutzman, Maria C G Juenger, and David W. Fowler. 2010. “Comprehensive Phase Characterization of Crystalline and Amorphous Phases of a Class F Fly Ash.” *Cement and Concrete Research* 40 (1): 146–56. https://doi.org/10.1016/j.cemconres.2009.08.029.

Chowdhury, Subrato, and Prabir C. Basu. 2010. “Strength-Cementitious Material-Water Relationship for Proportioning of Fly Ash-Based Concrete.” *ACI Materials Journal* 107 (4): 340–48.

Gesoğlu, Mehmet, Erhan Güneyisi, and Erdoğan Özbay. 2009. “Properties of Self-Compacting Concretes Made with Binary, Ternary, and Quaternary Cementitious Blends of Fly Ash, Blast Furnace Slag, and Silica Fume.” *Construction and Building Materials* 23 (5): 1847–54. https://doi.org/10.1016/j.conbuildmat.2008.09.015.

Hannesson, Guðmundur, Katherine Kuder, Rob Shogren, and Dawn Lehman. 2012. “The Influence of High Volume of Fly Ash and Slag on the Compressive Strength of Self-Consolidating Concrete.” *Construction and Building Materials* 30: 161–68. https://doi.org/10.1016/j.conbuildmat.2011.11.046.

Hemalatha, T., and Ananth Ramaswamy. 2017. “A Review on Fly Ash Characteristics – Towards Promoting High Volume Utilization in Developing Sustainable Concrete.” *Journal of Cleaner Production* 147: 546–59. https://doi.org/10.1016/j.jclepro.2017.01.114.

Jalal, Mostafa, Alireza Pouladkhan, Omid Fasihi Harandi, and Davoud Jafari. 2015.

"Comparative Study on Effects of Class F Fly Ash, Nano Silica and Silica Fume on Properties of High Performance Self Compacting Concrete." *Construction and Building Materials* 94: 90–104. https://doi.org/10.1016/j.conbuildmat.2015.07.001.

Khan, Inamullah, Arnaud Castel, and Raymond Ian Gilbert. 2017. "Effects of Fly Ash on Early-Age Properties and Cracking of Concrete." *ACI Materials Journal* 114 (4): 673–81. https://doi.org/10.14359/51689898.

Kuder, Katherine, Dawn Lehman, Jeffrey Berman, Gudmundur Hannesson, and Rob Shogren. 2012. "Mechanical Properties of Self Consolidating Concrete Blended with High Volumes of Fly Ash and Slag." *Construction and Building Materials* 34: 285–95. https://doi.org/10.1016/j.conbuildmat.2012.02.034.

Mamlouk, M.S., Zaniewski, J.P. 2006. "Materials for Civil and Construction Engineers." In *Second Edition, Pearson Prentice Hall, New Jersey*. https://the-eye.eu/public/WorldTracker.org/College Books/Materials for Civil and Construction Engineers/Materials for Civil and Construction Engineers 2e.pdf.

Mehta, P K. 1985. "INFLUENCE OF FLY ASH CHARACTERISTICS ON THE STRENGTH OF PORTLAND-FLY ASH MIXTURES." *CEMENT and CONCRETE RESEARCH*. Vol. 15. https://ac.els-cdn.com/0008884685900675/1-s2.0-0008884685900675-main.pdf?_tid=50648eff-3a6e-4100-a370-4f906cf306c8&acdnat=1542051730_762af222f3b29dddbb152b72e700fd6f.

Nguyen, Hoang Anh, Ta Peng Chang, Jeng Ywan Shih, Chun Tao Chen, and Tien Dung Nguyen. 2015. "Influence of Circulating Fluidized Bed Combustion (CFBC) Fly Ash on Properties of Modified High Volume Low Calcium Fly Ash (HVFA) Cement Paste." *Construction and Building Materials* 91: 208–15. https://doi.org/10.1016/j.conbuildmat.2015.05.075.

Oner, A, S Akyuz, and R Yildiz. 2005. "An Experimental Study on Strength Development of Concrete Containing Fly Ash and Optimum Usage of Fly Ash in Concrete." *Cement and Concrete Research* 35 (6): 1165–71.

https://doi.org/10.1016/j.cemconres.2004.09.031.

Papadakis, Vagelis G. 2000. “Effect of Fly Ash on Portland Cement Systems. Part II. High-Calcium Fly Ash.” *Cement and Concrete Research* 30 (10): 1647–54. https://doi.org/10.1016/S0008-8846(00)00388-4.

Poon, C S, L Lam, and Y L Wong. n.d. “A Study on High Strength Concrete Prepared with Large Volumes of Low Calcium Fly Ash.” Accessed September 30, 2018. https://ac.els-cdn.com/S0008884699002719/1-s2.0-S0008884699002719-main.pdf?_tid=3fffc292-07d0-4abd-8ca3-11a9fbb18724&acdnat=1538360090_95bf2051bad26f1cbbc28abc6dd6cd42.

Ravina, Dan, and P.K. Mehta. 1988. “COMPRESSIVE STRENGTH OF LOW CEMENT/HIGH FLY ASH CONCRETE.” *CEMENT and CONCRETE RESEARCH.* 18: 571–83.

Saha, Ashish Kumer. 2018. “Effect of Class F Fly Ash on the Durability Properties of Concrete.” *Sustainable Environment Research* 28 (1): 25–31. https://doi.org/10.1016/j.serj.2017.09.001.

Shi, Caijun, and Robert L Day. 2000. “Pozzolanic Reaction in the Presence of Chemical Activators: Part II. Reaction Products and Mechanism.” *Cement and Concrete Research* 30 (4): 607–13. https://doi.org/10.1016/S0008-8846(00)00214-3.

Siddique, Rafat. 2004. “Performance Characteristics of High-Volume Class F Fly Ash Concrete.” *Cement and Concrete Research*. https://doi.org/10.1016/j.cemconres.2003.09.002.

———. 2011. “Properties of Self-Compacting Concrete Containing Class F Fly Ash.” *Materials and Design* 32 (3): 1501–7. https://doi.org/10.1016/j.matdes.2010.08.043.

Sumer, Mansur. 2012. “Compressive Strength and Sulfate Resistance Properties of Concretes Containing Class F and Class C Fly Ashes.” *Construction and Building Materials* 34: 531–36. https://doi.org/10.1016/j.conbuildmat.2012.02.023.

Tait, Michael W., and Wai M. Cheung. 2016. “A Comparative Cradle-to-Gate Life Cycle Assessment of Three Concrete Mix Designs.” *International Journal of Life Cycle Assessment*. https://doi.org/10.1007/s11367-016-1045-5.

Tokyay, M. 1999. “Strength Prediction of Fly Ash Concretes by Accelerated Testing.” *Cement and Concrete Research*. Vol. 29. https://ac.els-cdn.com/S000888469900160X/1-s2.0-S000888469900160X-main.pdf?_tid=ac888bb4-2136-4e3c-b046-aae810ff85ca&acdnat=1542051046_1a4feef92517002184c5025cc65f72a5.

Ward, Colin R., and David French. 2006. “Determination of Glass Content and Estimation of Glass Composition in Fly Ash Using Quantitative X-Ray Diffractometry.” *Fuel* 85 (16 SPEC. ISS.): 2268–77. https://doi.org/10.1016/j.fuel.2005.12.026.

Wongkeo, Watcharapong, Pailyn Thongsanitgarn, Athipong Ngamjarurojana, and Arnon Chaipanich. 2014. “Compressive Strength and Chloride Resistance of Self-Compacting Concrete Containing High Level Fly Ash and Silica Fume.” *JOURNAL OF MATERIALS&DESIGN* 64: 261–69. https://doi.org/10.1016/j.matdes.2014.07.042.

Xu, Gang, and Xianming Shi. 2018. “Characteristics and Applications of Fly Ash as a Sustainable Construction Material: A State-of-the-Art Review.” *Resources, Conservation and Recycling* 136 (April): 95–109. https://doi.org/10.1016/j.resconrec.2018.04.010.

Yao, Z. T., X. S. Ji, P. K. Sarker, J. H. Tang, L. Q. Ge, M. S. Xia, and Y. Q. Xi. 2015. “A Comprehensive Review on the Applications of Coal Fly Ash.” *Earth-Science Reviews*. https://doi.org/10.1016/j.earscirev.2014.11.016.

APPENDIX A: DATASET INFORMATION

Dataset Information

	Min.	Max.	Mean	Std. Dev.
28 day str	5.80	92.13	40.70	18.68
w/c	0.26	4.00	0.70	0.41
w/b	0.19	0.94	0.43	0.16
% replacement	5.00	90.00	32.98	17.26
SiO2	30.50	68.40	52.23	8.95
Al2O3	13.00	32.55	23.99	4.90
Fe2O3	3.10	20.60	6.36	2.95
CaO	0.30	28.60	9.28	8.53
MgO	0.00	7.50	1.86	1.67
SO3	0.07	4.60	1.24	1.39
Na2O	0.00	3.60	0.85	0.88
K2O	0.00	3.80	1.48	1.35
TiO2	0.00	1.30	0.09	0.26
P2O5	0.00	0.21	0.02	0.06
LOI	0.00	4.50	1.35	1.12
Big 3 oxides	54.10	95.26	82.59	11.11

Sources of data for model: (Siddique 2011)(Wongkeo et al. 2014)(Jalal et al. 2015)(Chowdhury and Basu 2010)(Kuder et al. 2012)(Poon, Lam, and Wong n.d.)(Oner, Akyuz, and Yildiz 2005)(Siddique 2004)(Hannesson et al. 2012)(Bouzoubaâ and Lachemi 2001)(Papadakis 2000)(Burris and Riding 2014)(Mehta 1985)(Ravina and Mehta 1988)(Tokyay 1999)

APPENDIX B: XRD SCANS

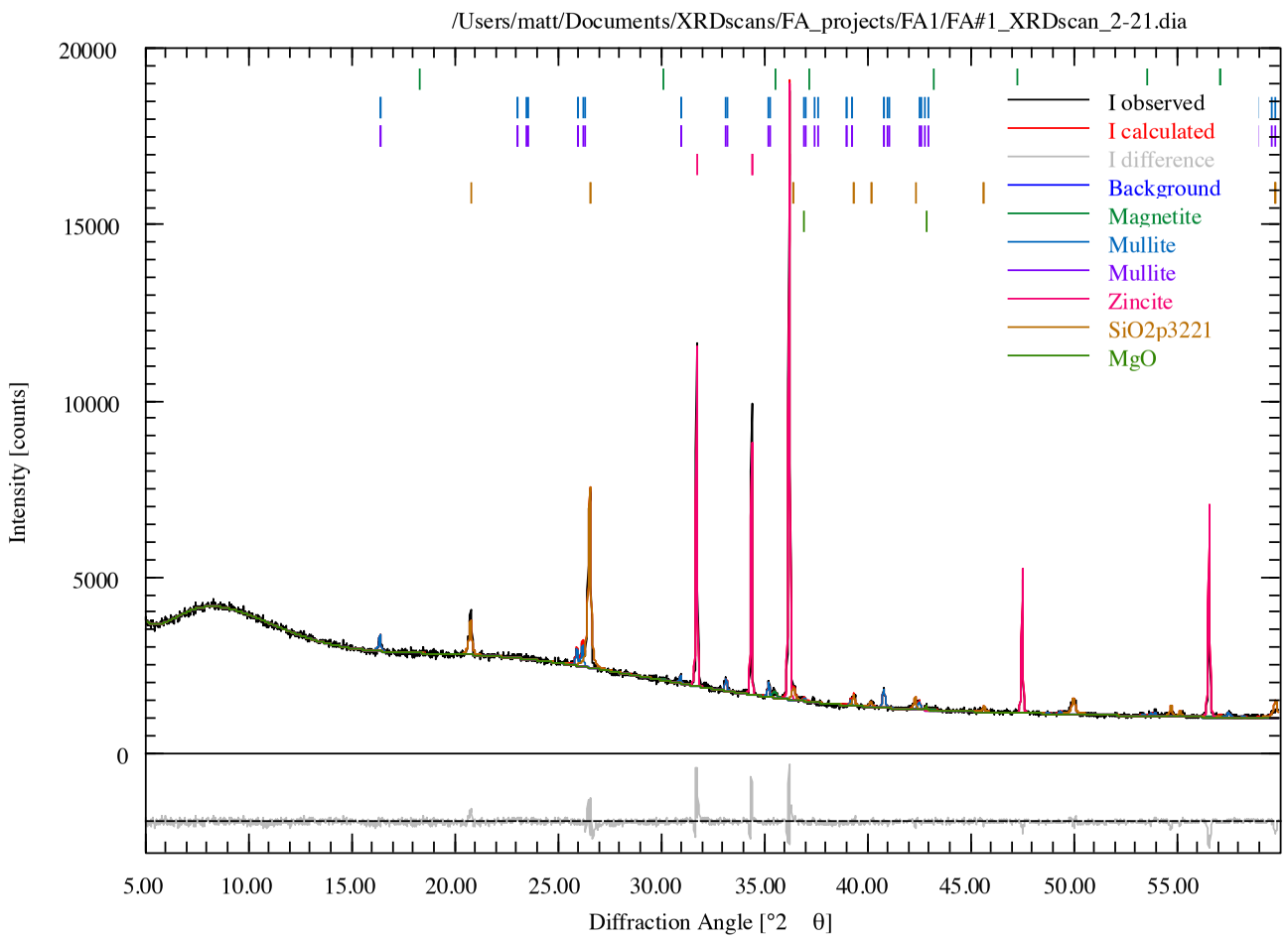
/Users/matt/Documents/XRDscans/FA_projects/FA1/FA#1_XRDscan_2-21.dia
I observed
I calculated
I difference
Background
Magnetite
Mullite
Mullite
Zincite
SiO2p3221
MgO
Intensity [counts]
20000
15000
10000
5000
0
5.00
10.00
15.00
20.00
25.00
30.00
35.00
40.00
45.00
50.00
55.00
Diffraction Angle [°2 θ]

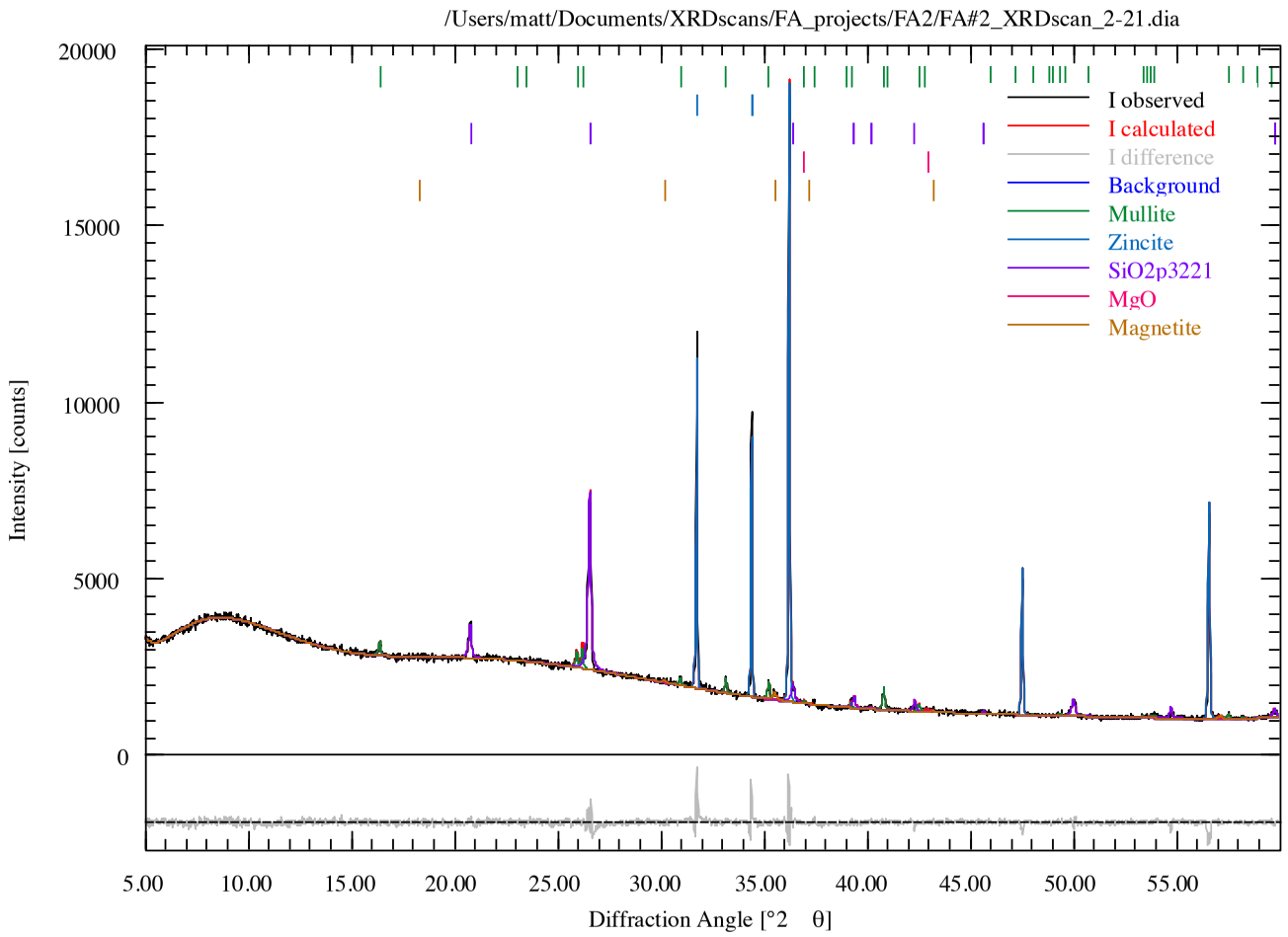
/Users/matt/Documents/XRDscans/FA_projects/FA2/FA#2_XRDscan_2-21.dia
I observed
I calculated
I difference
Background
Mullite
Zincite
SiO2p3221
MgO
Magnetite
Intensity [counts]
20000
15000
10000
5000
0
5.00
10.00
15.00
20.00
25.00
30.00
35.00
40.00
45.00
50.00
55.00
Diffraction Angle [°2 θ]

09

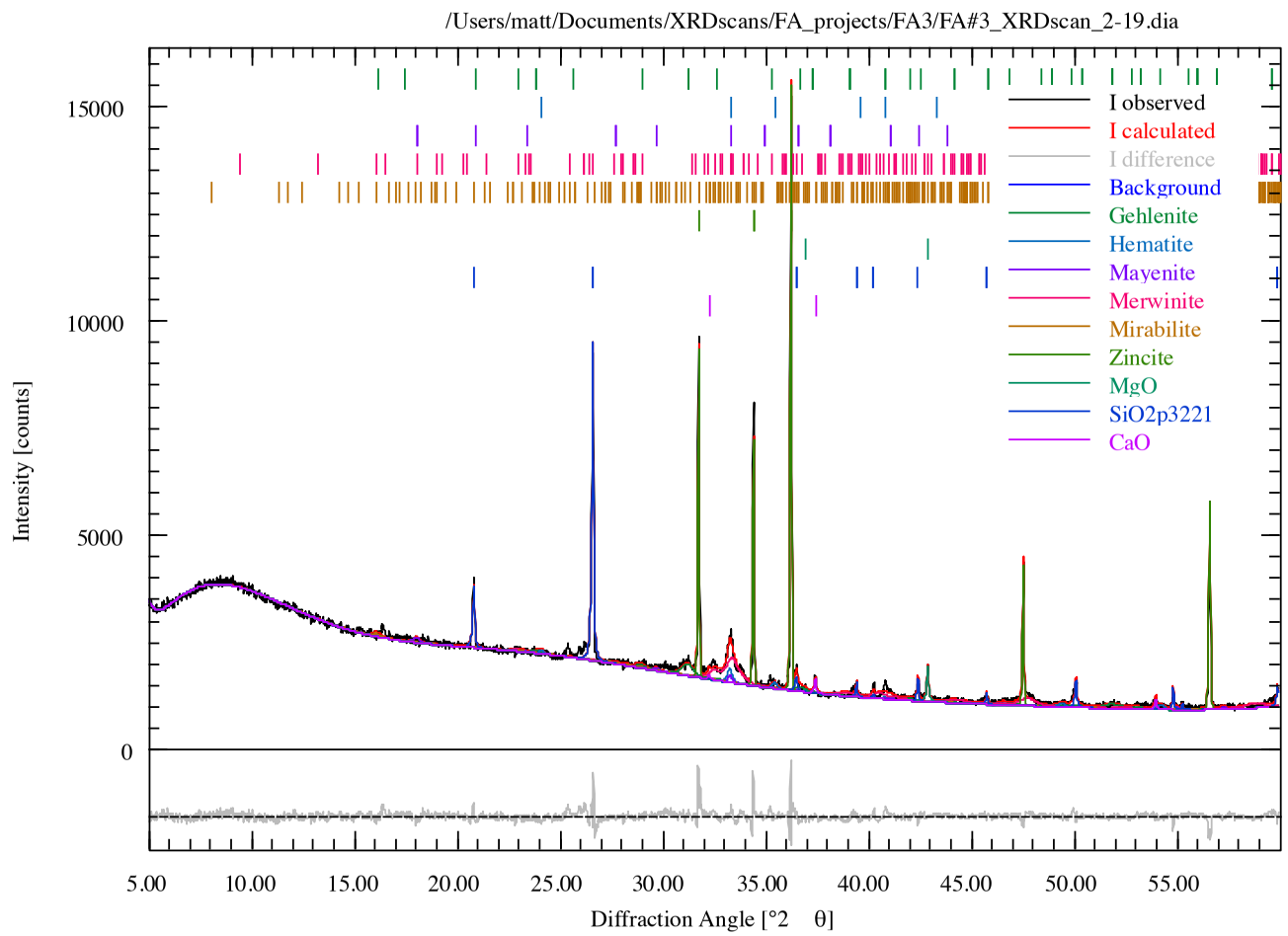
/Users/matt/Documents/XRDscans/FA_projects/FA3/FA#3_XRDscan_2-19.dia
I observed
I calculated
I difference
Background
Gehlenite
Hematite
Mayenite
Merwinite
Mirabilite
Zincite
MgO
SiO2p3221
CaO
Intensity [counts]
15000
10000
5000
0
5.00
10.00
15.00
20.00
25.00
30.00
35.00
40.00
45.00
50.00
55.00
Diffraction Angle [°2 θ]

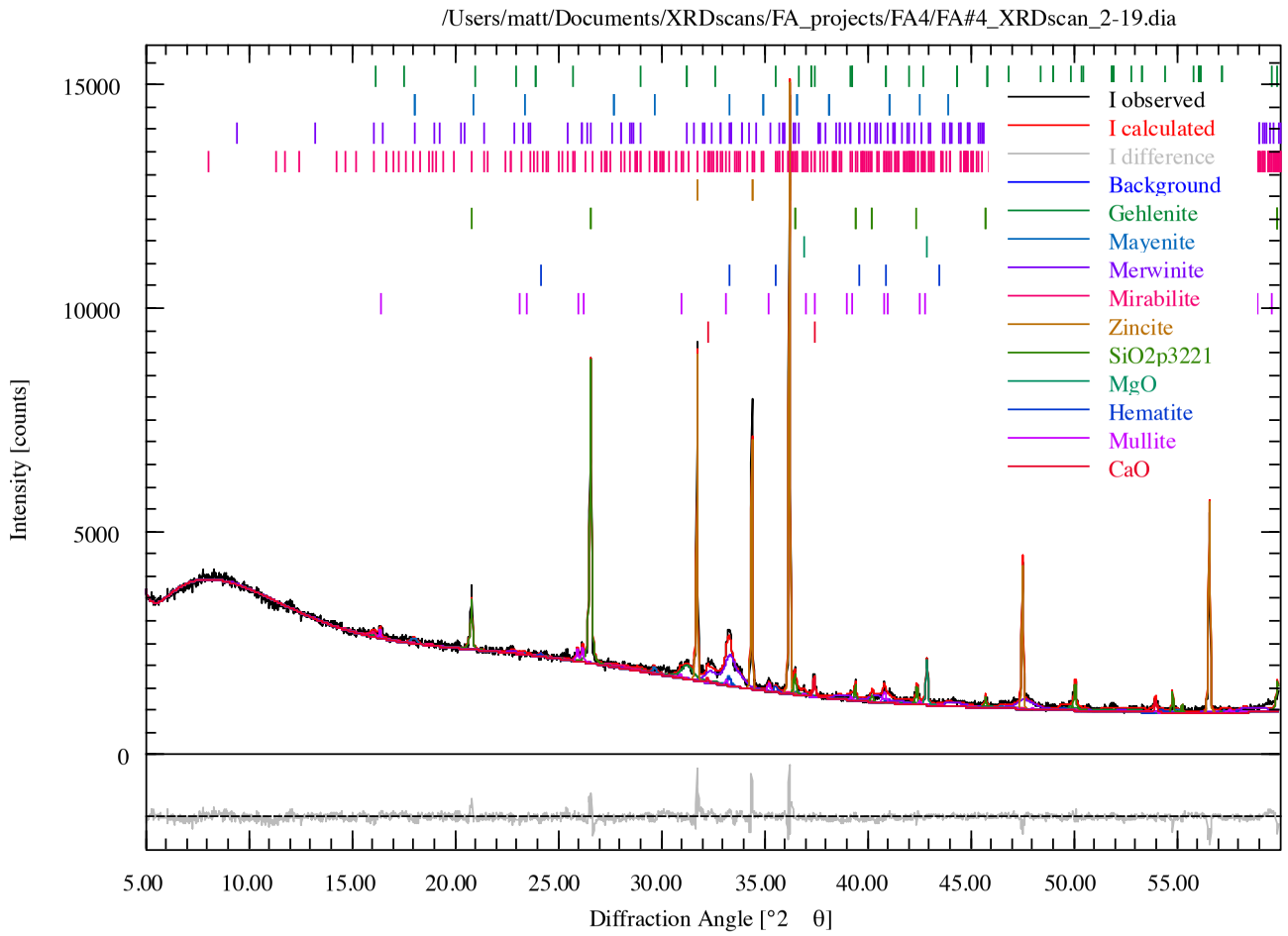
/Users/matt/Documents/XRDscans/FA_projects/FA4/FA#4_XRDscan_2-19.dia
Intensity [counts]
15000
10000
5000
0
5.00
10.00
15.00
20.00
25.00
30.00
35.00
40.00
45.00
50.00
55.00
Diffraction Angle [°2 θ]
I observed
I calculated
I difference
Background
Gehlenite
Mayenite
Merwinite
Mirabilite
Zincite
SiO2p3221
MgO
Hematite
Mullite
CaO

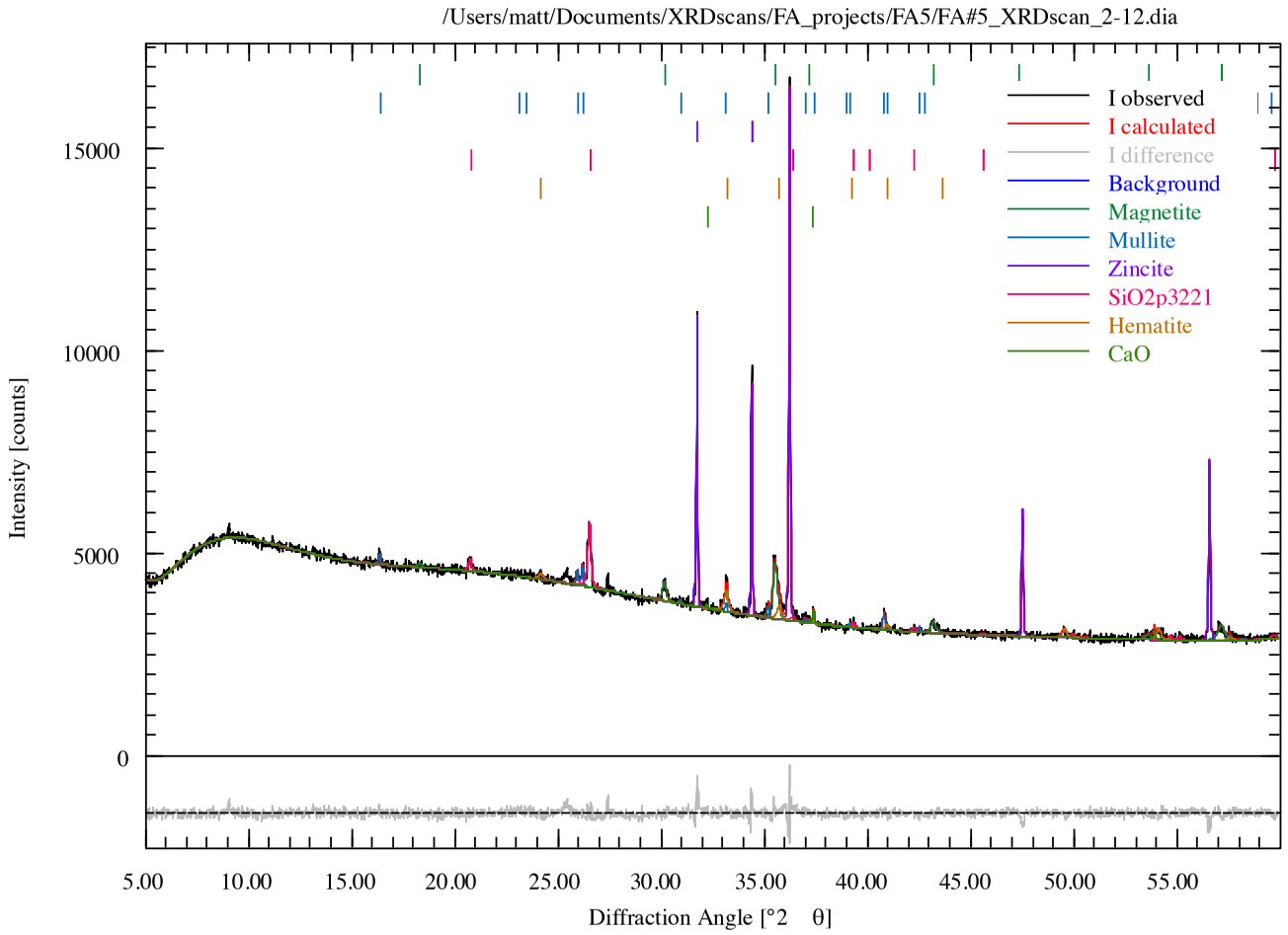
/Users/matt/Documents/XRDscans/FA_projects/FA5/FA#5_XRDscan_2-12.dia
I observed
I calculated
I difference
Background
Magnetite
Mullite
Zincite
SiO2p3221
Hematite
CaO
Intensity [counts]
15000
10000
5000
0
5.00
10.00
15.00
20.00
25.00
30.00
35.00
40.00
45.00
50.00
55.00
Diffraction Angle [°2 θ]

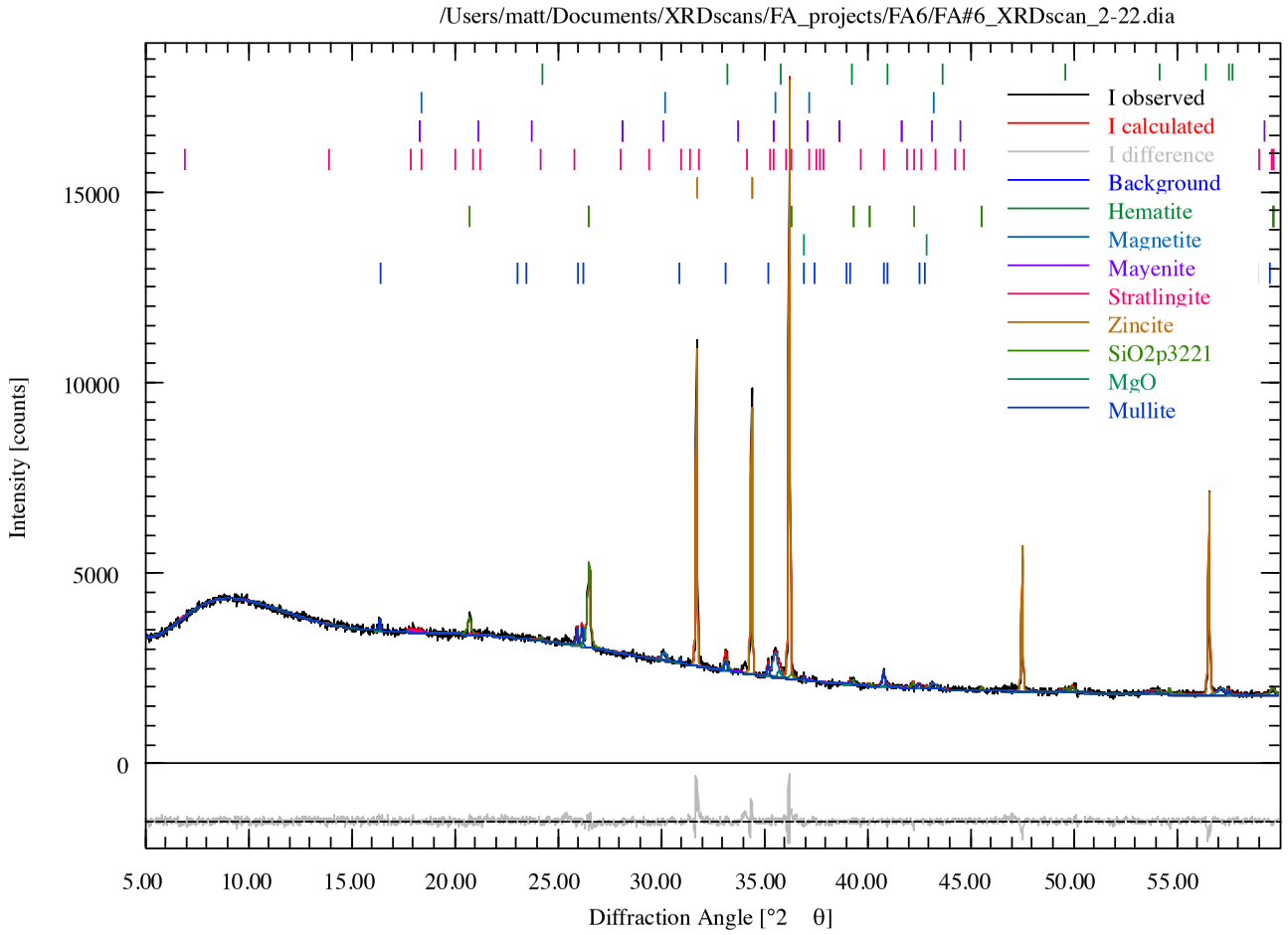
/Users/matt/Documents/XRDscans/FA_projects/FA6/FA#6_XRDscan_2-22.dia
I observed
I calculated
I difference
Background
Hematite
Magnetite
Mayenite
Stratlingite
Zincite
SiO2p3221
MgO
Mullite
Intensity [counts]
15000
10000
5000
0
5.00
10.00
15.00
20.00
25.00
30.00
35.00
40.00
45.00
50.00
55.00
Diffraction Angle [°2 θ]